Routing, Core, Modulation Level, and Spectrum Assignment Based on Image Processing Algorithms

Pedro M. Moura and Nelson L. S. da Fonseca

***Abstract*—This paper proposes four algorithms for routing, core, modulation level, and spectrum assignment (RCMLSA) based on image processing to search for the available spectrum of multicore fibers at low computational cost. The solutions aim at efficiently utilizing the optical spectrum by considering the crosstalk between the cores of network fibers, as well as by avoiding the allocation of lightpaths that degrade the optical signal. Lightpaths are thus allocated employing the highest possible level of modulation. The results show that the proposed algorithms can decrease the blocking ratio by four orders of magnitude when compared with other RCMLSA algorithms in the literature.**

***Index Terms*—Crosstalk; Elastic optical networks; Modulation; Space division multiplexing.**

I. Introduction

The past decade has seen a tremendous growth in the use of Internet applications with diverse requirements. Some of the applications have low bandwidth requirements, whereas for others, such as high-resolution video, these requirements are high [1]. These heterogeneous demands can be dealt with using elastic (flexgrid) optical network technology since it uses a fine-grained allocation of the spectrum, and advanced transmission techniques such as orthogonal frequency-division multiplexing and Nyquist-pulse shape. These technologies lead to greater efficiency in spectrum allocation and a reduction in the wastage of resources when compared with the traditional wavelength-division multiplexing technology [2–4].

Despite the benefits of this new technology, the capacity of optical networks is expected to reach its physical limitations in the near future. One of the proposals for the expansion of this capacity is space-division multiplexing (SDM) [5] employing multicore fibers (MCFs), since there are several independent cores in a single-fiber cable, which can be treated as single-core fibers [6–8].

However, in these MCFs, physical intercore crosstalk (XT) occurs because of core coupling and their disposition. However, low XT can be achieved with up to 22 cores if the spectrum allocation is adequate [9–11].

To further increase the transmission efficiency, a variety of modulation formats can be employed. Although a larger number of bits per symbol increases the transmission sensitivity to degradation [12], the modulation level, which depends on the physical distance, must be chosen carefully so that the signal can be correctly decoded at the destination, considering the XT intensity [13].

The routing, modulation level, and spectrum assignment (RMLSA) problem in elastic optical networks consists of finding a route, a modulation level, and an available spectrum for the establishment of a lightpath. This allocation is subject to both continuity and contiguity constraints. The former requires that the set of slots assigned by an algorithm must be the same for all links along a route, to avoid opto-electrical conversion of the optical signal, whereas the latter guarantees that the slots allocated are contiguous, so that high spectrum efficiency can be obtained. In general, RMLSA algorithms identify the potential sequence of slots that satisfy the bandwidth requested and apply specific criteria to choose one from the potential sequences of slots [14–16].

In SDM optical networks, this problem can also be extended to allocate cores for the establishment of a lightpath, known as the routing, core, modulation level, and spectrum assignment (RCMLSA) problem. The addition of the space dimension increases the computational complexity of the spectrum allocation procedure, since spectra in all cores have to be taken into consideration during the computation of routes. The XT generated by coupled fibers also impacts the modulation level directly, since sensitivity to interference increases with the number of bits per symbol transmitted. Moreover, its effect must be considered on not only the lightpath being allocated, but also others established already [17,18].

Recent studies [19–22] considering the impact of XT on slot availability in elastic optical networks with SDM have proposed algorithms employing fixed modulation levels, chosen only on the basis of the physical distance and assuming worst-case XT values. Such an approach will lead to the employment of conservative levels of modulation. The scheme introduced in this paper copes with these problems by choosing the modulation level on the basis of the estimated XT in the fiber cores. This paper considers a

Manuscript received July 23, 2018; revised September 11, 2018; accepted September 13, 2018; published October 18, 2018 (Doc. ID 340385).

P. M. Moura (e-mail: pedrom@lrc.ic.unicamp.br) and N. L. S. da Fonseca are with Computer Networks Laboratory, Institute of Computing, State University of Campinas, Campinas, Brazil.

https://doi.org/10.1364/JOCN.10.000947

variety of traffic scenarios, a precise model for the estimation of XT, and the adjustment of the modulation level according to the estimated XT, yet is capable of maintaining low computational complexity for the RCMLSA algorithm.

The contribution of this paper is the introduction of four novel RCMLSA algorithms, which adopt a new approach for the identification of potential sequences of allocable slots and select one of them. For the identification of sequences of available slots on a selected route, their spectra are represented as a matrix, in which the number of cores is represented on one dimension and the number of slots on the other. Such a representation makes it possible to use algorithms developed for 2D binary image processing to identify sequences of available slots. Two different image processing algorithms are used in this paper, namely connected component labeling (CCL) and the inscribed rectangles algorithm (IRA). Both algorithms reduce the computational complexity of the RCMLSA algorithms. The algorithms proposed here are designed for networks with optical switches, but without lane (core) changes, the transmission is carried out in the same cores along the chosen path.

The results indicate that the proposed algorithms can achieve blocking ratios up to four orders of magnitude lower than those obtained using other existing algorithms. This is the result of allocation of lightpaths considering XT, thus making it possible to use a higher level of modulation and allocate fewer slots per lightpath, consequently increasing the number of concurrent lightpaths in the network. Despite the high number of variables that an RCMLSA algorithm must consider, the algorithms proposed here are able to maintain low computational complexity due to the use of image processing algorithms to identify slot availability, thus making the algorithms feasible for adoption in real networks.

This paper is organized as follows: Section II presents some related work. Section III presents the image processing algorithms employed. Section IV presents a model for the estimation of the XT value. Section V describes the proposed algorithms, fitting policies, and how they work together. Section VI provides some numerical examples and compares the proposed algorithms with an integer linear programming (ILP) solution from the literature. Section VII draws some conclusions about the proposed algorithms.

II. Related Work

In Ref. [7], an overview of possible SDM approaches focusing on network planning was provided. The paper introduced the RCMLSA problem (called RSMLSA by the authors) and listed the challenges arising from the use of the space dimension. Network control frameworks were also presented to encourage the usage of centralized solutions based on software-defined networks and path computation elements.

In Ref. [5], a dynamic RCMLSA algorithm was proposed to reduce both XT and fragmentation. The former adopts a policy called core prioritization to avoid simultaneous allocation of coupled cores of the MCF. The latter adopts a policy called core classification to reduce fragmentation by allocating lightpaths with the same bandwidth in the same core, mitigating the probability of fragmentation caused by the establishment and termination of lightpaths. The results indicate that these policies reduce XT and blocking under various network conditions.

Estimating intercore XT in MCFs is a complex task, due to its statistical behavior. In Ref. [23], an analytical expression for the average power coupling coefficient was proposed. The expression is based on an exponential autocorrelation function, which reduces the mathematical and computational complexities. The results indicate that the values estimated using this expression match those obtained using other more complex functions.

In Ref. [24], an ILP formulation for the static routing, core, and spectrum assignment (RCSA) problem was introduced to minimize the number of slots allocated by evaluating the number of spectrum slots required to accommodate a given set of traffic demands, and considering requirements such as intercore XT and spectrum overlapping. Given the high computational complexity of the ILP, a heuristic was proposed for a sub-optimal, but scalable, solution. The results indicate that the heuristic closely approximates the optimal solution given by the ILP.

In Refs. [25] and [26], two simple RCSA algorithms were proposed employing image processing to represent the link spectra. The algorithms proposed in this paper differ from those in Refs. [25] and [26] by including XT estimations and different modulation levels. The aim is to maximize the use of the spectrum and prevent XT interference, which degrades the received optical signal.

In Ref. [19], a spectrum and core assignment algorithm is proposed to allocate cores and slots of the spectrum considering different modulation formats and XT estimations. However, the proposed algorithm was designed to make the allocation on a single link, rather than on a multi-hop basis. A greedy heuristic algorithm for static RCSA was introduced in Ref. [27] and employed jointly with the proposed models for the calculation of intercore XT and transmission reach; various modulation formats were employed. These models, however, assume worst-case XT thresholds for transmission based on path distances.

In Ref. [20], models for the calculation of intercore XT and transmission reach are studied, with worst-case XT thresholds employed for choosing the modulation formats. The greedy heuristic algorithm for static RCSA from Ref. [27] is used to evaluate the models.

A XT-aware heuristic for the RCSA problem is proposed in Ref. [21]; it estimates the XT and tries to avoid allocations that could lead to incorrect decoding of the optical signal at the destination. Although the algorithm is able to reduce the number of lightpaths affected by XT, it does not leverage on the possibility of adjusting the modulation format according to the estimated XT.

In Ref. [22], real XT values were reported from prototype experiments. The values were used to estimate the

worst-case transmission reach of the optical signal, employing various bit rates and modulation formats, considering the intercore XT produced by simultaneous utilization of several cores. The results were validated using an ILP formulation as well as a heuristic algorithm, considering transmission reach constraints. The algorithms used fixed modulation formats chosen as a function of the distance to the destination.

The present paper differs from those described above by proposing RCMLSA algorithms for a dynamic network scenario. These algorithms select the highest possible modulation level considering the estimated XT in the network fibers when a request arrives. The proposed algorithms lead to high efficiency in resource allocation and maintain low computational complexity.

The solutions proposed in Refs. [19–22] for the RCSA problem assumed static network scenarios, as well as previous knowledge about the arrival of all requests for the establishment of connections. Such assumptions allow the optimization of RCSA allocations that avoid XT, since it is possible to evaluate how a lightpath to be established will interfere with others. However, such assumptions are less realistic than those employed in the present paper, which do not assume previous knowledge about the arrival of requests. This paper differs from Ref. [19] in that the spectrum is allocated along the lightpaths, rather than on a single link. It differs from Refs. [20,22] by the estimation of XT values at the time of potential allocation, rather than considering a predefined worst-case XT value. Moreover, it differs from Ref. [21] in that the highest possible modulation level for the allocation of a lightpath is chosen on the basis of the estimated XT at the time of allocation, thus attempting to increase the spectrum efficiency.

III. Spectrum Availability

Two image processing algorithms for searching for an available spectrum are used in this paper: connected component labeling (CCL) and the inscribed rectangles algorithm (IRA). The former finds images of any shape, whereas the latter identifies only rectangles. If, on the one hand, CCL identifies a larger number of allocable regions in the spectrum, on the other, the IRA provides information about allocable regions with shapes of interest.

A. Connected Component Labeling

The CCL algorithm is fundamental in the pattern analysis of digital images, where labeling is essential, such as fingerprint identification, character recognition, and medical image analysis, to name a few. The goal of CCL is to discover objects in an image by analyzing the connectivity of the pixels of that image. CCL can use different connectivity models: the 4-connectivity, which considers objects formed by horizontally and vertically connected pixels, and the 8-connectivity, which also considers diagonally connected pixels [28]. Figure 1 illustrates the output of a 4-connectivity-based CCL algorithm. In this figure, background pixels are labeled 0, whereas objects with connected pixels are labeled either 1 or 2, thus distinguishing the two different regions found by the algorithm.

The use of the CCL algorithm to identify allocable regions in the spectrum helps reduce the computational complexity of the RCSA algorithm. The connected regions satisfy the contiguity constraint for spectrum allocation.

The output image, Fig. 1, is transformed into a set of regions of contiguous slots with their coordinates forming a matrix that represents the spectrum. Such a representation facilitates the choice of regions in relation to size, format, and location.

In Ref. [29], optimization techniques are proposed to decrease the computational complexity of the CCL algorithm. The number of operations is decreased by representing the image as a decision tree. A streamlined union-find technique is also proposed to reduce the number of operations.

The CCL algorithm is divided into two steps, namely the scan and labeling phases. The former is responsible for iterations over the connected pixels numerically marked as 0, whereas the latter is responsible for labeling of the pixels into separated regions.

Two different approaches can be employed in the scanning step of the CCL algorithms: one-scan and two-scan. The one-scan approach scans and labels in a single step [30] and supports 4 and 8 connectivities. It is recommended for images containing large numbers of objects. The two-scan approach [31] utilizes two different steps. In the first step, provisional labels are assigned; these are replaced in the second scan by the final label. The two-scan algorithm requires an additional data structure to store the provisional labels; however, since memory limitation is not an issue, this approach demands lower computational complexity than the other.

The two-scan approach is employed by the RCMLSA algorithms proposed here.

B. Inscribed Rectangles Algorithm

The IRA finds rectangular shapes consisting of connected pixels [32]. Figure 2 illustrates the identification

0	0	0	0	0	0	0	0	0	0	0	0	0	0	0	0
0	1	1	1	1	1	1	1	1	0	0	0	0	0	0	0
0	1	1	1	1	1	1	1	1	0	0	0	0	0	0	0
0	1	1	1	1	1	1	1	1	0	0	0	0	0	0	0
0	1	1	1	1	1	1	0	0	0	0	0	0	0	0	0
0	1	1	1	1	1	1	0	0	0	0	0	0	0	0	0
0	1	1	1	1	1	1	0	0	0	0	0	0	0	0	0
0	0	0	0	1	1	1	0	0	0	0	0	0	0	0	0
0	0	0	0	0	0	0	0	0	0	0	0	0	0	0	0
0	0	0	0	0	0	0	0	0	0	0	0	0	2	0	
0	0	0	0	0	0	0	2	2	2	2	2	2	2	0	
0	0	0	0	0	0	0	2	2	2	2	2	2	2	0	
0	0	0	0	0	0	0	2	2	2	2	2	2	2	0	
0	0	0	0	0	0	0	2	2	2	2	2	2	2	0	
0	0	0	0	0	0	0	2	2	2	0	0	0	0	0	

Fig. 1. Labeled binary image—output of a CCL algorithm.

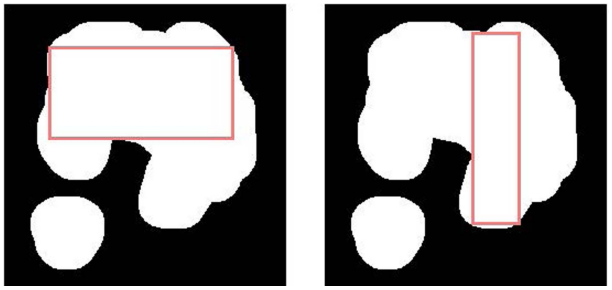

Fig. 2. Rectangles inscribed inside a shape.

of two different rectangles inside the connected shapes identified.

The IRA furnishes a set of all possible distinct rectangles inside an image as output. This is quite useful for the RCMLSA problem since the size and coordinates of the rectangles, as well as their shapes, can be exploited to develop solutions for the amelioration of problems caused by the use of the space dimension, such as XT and fragmentation. Figure 2 presents two examples of rectangles inscribed inside a binary image.

For the RCMLSA problem, wider rectangles should be prioritized, since they divide the lightpaths into a fewer cores, thus requiring fewer band guards and causing less XT between the coupled cores.

The IRA is based on the largest rectangle algorithm [33], which divides the problem into smaller sub-problems by first finding smaller squares and combining them into larger ones, as is common in dynamic programming solutions.

A mask matrix M of the same size as the image is created; it is then filled bottom-up and right to left based on the following rules: pixels presenting neighbors previously marked with a value of 0 are marked with a value of 1 in M. For pixels with neighbors with values larger than 0, the following equation is used to define the value of M:

$$M_{i,j} = \min(M_{i+1,j}, M_{i,j+1}, M_{i+1,j}) + 1. \quad (1)$$

At the end of the process, an array containing the coordinates of all possible rectangles will be created. To transform this array into a set, the rectangles contained within other rectangles (with higher initial pixel and lower ending pixel) must be eliminated; this is achieved by not adding them to the new set.

IV. Physical Impairment Estimation on MCFs

To avoid interference between lightpaths and, consequently, the degradation of their optical signals, an estimation of the physical impairments must be made before any allocation on a spectrum. Some impairments, such as chromatic dispersion and polarization mode dispersion, can be solved by digital signal processing on coherent receivers. Having addressed these impairments, intercore XT has become the major concern when using MCFs [34].

A minimum signal-to-noise ratio (SNR) value should be met to assure quality of transmission (QoT), so that a signal can be correctly decoded at the destination, assuming a bit error correction is employed. Those values are dependent on the modulation format employed, since different bit per symbol rates have different sensitivities to interference.

Three conditions must be verified in order to classify a slot as available for allocation: (i) the slot must not be allocated for another lightpath; (ii) the SNR on the corresponding slot must not be lower than a certain threshold value; and (iii) a lightpath to be established containing the slot must not generate unacceptable levels of XT on the slots of other existing lightpaths of a coupled fiber core. A binary matrix called availability matrix (A^m_{uv}) is employed in the proposed algorithms. Its elements have a value of 1 when the correspondent slot is available, and 0 otherwise. Those values are updated at every new lightpath establishment or tear down. When a lightpath request arrives, a modulation format is chosen considering the maximum transmission reach achievable as a function of the estimated aggregated XT.

Equation (2) defines the availability matrix A^m_{uv} for a specific modulation level m, considering the noise level generated by XT in a link between nodes u and v:

$$A^m_{uv} = [a_{ij}] = \begin{cases} 1 & (s_{ij} = 1) \wedge (P - n_{ij} \geq T_m) \wedge (d_{ij} = 0) \\ 0 & \text{otherwise} \end{cases}, \quad (2)$$

$$N_{uv} = [n_{ij}] = \sum_{c \in C_i} XT_t | s_{cj} = 1, \quad (3)$$

$$D^m_{uv} = [d_{ij}] = \begin{cases} 1 & \forall\, c \in C\ P - n_{cj} \geq T_m \\ 0 & \text{otherwise} \end{cases}. \quad (4)$$

Here, $S_{uv} = [s_{ij}]$ is the occupancy matrix, with i being the ith core and j being the jth slot of the spectrum; element s_{ij} is 1 if slot (i,j) in the link uv is available for allocation, and 0 otherwise; $N_{uv} = [n_{ij}]$ is the noise matrix, whose element n_{ij} gives the estimated XT on slot (i,j) in the link uv; $D^m_{uv} = [d_{ij}]$ is the disruption matrix, whose element d_{ij} has a value of 1 if the SNR on slot (i,j) in the link uv is above certain threshold value in case an incoming lightpath is established, and 0 otherwise; $C_f = c$ represents coupled fiber cores of the fth core, a function of the MCF architecture; T_m is the SNR threshold for the modulation m to be correctly decoded at the destination; P is the transmission power in dB; and XT_t is the intercore XT value in dB, where t is the number of cores in the MCF.

The values used to calculate the elements of the matrices, as shown in the equations, are presented in Ref. [22]. Table I shows the worst-case scenarios of intercore XT (XT_t) for 7 cores [9], 12 cores [11], and 19 cores [10]. The XT_t value is defined on the basis of the distance between neighboring cores, which will be different for each value of t.

A list of empirical values is provided in Ref. [34], where a threshold (T_m) for correct decoding of a transmission for

TABLE I
INTERCORE XT (XT_t)

7 Cores	12 Cores	19 Cores
−84.7 dB	−61.9 dB	−54.8 dB

TABLE II
SNR AT BER 10^{-2} (T_m)

BPSK	QPSK	16-QAM	64-QAM
4.2 dB	7.2 dB	13.9 dB	19.8 dB

four levels of modulation [considering a bit error rate (BER) of 10^{-2}]: BPSK (1 bps), QPSK (2 bps), 16-QAM (4 bps), and 64-QAM (6 bps). Table II presents those values.

A maximum transmission reach is also calculated in Ref. [22], for several bit rates and fibers with 7, 12, and 19 cores. Considering the use of all the cores, the transmission reach will be limited by both signal attenuation and the aggregated XT coming from the coupled cores. Equation (5) gives the maximum distance for a modulation format m; the optical signal can be correctly decoded as a function of signal attenuation and the parameters of the MCF fiber architecture. Equation (6) gives the same distance but considering the aggregated XT along path p on the jth slot of the ith core. Equation (7) defines the maximum transmission distance achievable (in km):

$$\phi^m = \frac{P_s \cdot L_{\text{span}}}{T_m \cdot h \cdot f \cdot G \cdot NF \cdot R_s}, \tag{5}$$

$$\gamma_{ij}^m(p) = 10\frac{\sum_{e_{uv}\in p} n_i j - \rho_m}{10}, \tag{6}$$

$$MD_{ij}^m(p) = \min\{\phi, \gamma_{ij}^m(p)\}. \tag{7}$$

Here, $P_s = 1$ mW is the average optical power per channel; $L_{\text{span}} = 100$ km is the distance between equally spaced amplifiers; h is Planck's constant; f is the optical signal frequency; $G = 20$ dB is the amplifier gain; NF $= 5.5$ dB is the noise factor of the amplifiers; R_s is the symbol rate, including a coding overhead of 20% using forward error correction; and ρ_m is the fiber intercore XT for modulation format m in 1 km (BPSK, −14 dB; QPSK, −17 dB; 16-QAM, −23 dB; 64-QAM, 29 dB).

These estimations are used to calculate the XT present in the slots of an optical spectrum to determine the highest modulation level that should be employed for the requested lightpath allocation.

V. PROPOSED RCMLSA ALGORITHMS

An RCMLSA algorithm chooses route (path), slots, and cores to be allocated and the modulation level to be used. The number of slots necessary to satisfy the bandwidth demand depends on the modulation level chosen.

The algorithms proposed in this paper employ an image processing algorithm to identify the allocable slots and cores that satisfy the demand. A fitting policy chooses a single set of slots that will be chosen from the allocable ones identified by the image processing algorithm. Four algorithms are defined by the use of the CCL and IRA algorithms with different fitting policies. These four algorithms are derived from the meta Image-RCMLSA algorithm presented as Algorithm 1.

The Image-RCMLSA consists of four steps: initially, the candidate paths are calculated by employing the K-Shortest Path (KSP) algorithm. In the second step, the resultant spectrum matrices for each path and each modulation are created, as a function of the estimated XT. In the third step, an image processing algorithm is run to search for available portions of the spectrum. In the last step, a fitting policy chooses the slots on which the lightpath will be established.

The matrices resulting from the second step are calculated in two steps. Figure 3(a) illustrates the calculation of the availability matrix A_{uv}^m, obtained by performing a logical *AND* operation among the occupancy, noise, and disruption matrices. Figure 3(b) illustrates the second step, which is the calculation of the path spectrum matrix R resulting from the computation of a logical *AND* operation between all availability matrices along a path P. The darker elements of the matrices represent unavailable slots, whereas the lighter ones represent available slots. The path spectrum matrix R represents the availability of the spectra along the links of the paths for each modulation level, and will be used as input for the image processing algorithms.

Following notations will be used to describe the algorithm:

- s, source node;
- d, destination node;
- b, bandwidth demand in slots;
- c, number of cores in the MCFs;
- $r(s,d,b)$, request from node s to node d with a bandwidth demand of b;
- $m \in M$, modulation level. In this paper, the set considered is $M = \{1,2,4,6\}$, which corresponds to the number of bits per symbol for each modulation level;
- $b_m = \frac{b}{m} \times c$, number of slots needed to allocate a bandwidth of b using modulation m;
- $G = (V,E,S)$, network graph composed of a set of nodes V, a set of edges E, and a set of occupancy matrices S, associated with the edges of the graph;
- $E = \{e_{uv}\}$, set of edges e_{uv} connecting u and v in G;
- s_{ij}, occupancy matrix representing the spectrum of the link between u and v in G;
- $P = \{p_k\}$, set of paths resulting from the KSP algorithm;
- $\delta(p_k)$, physical distance between the source and destination along path p_k;

L_k^m, set of regions of the spectrum—output of the image processing algorithm;
R_k^m, path spectrum matrix—obtained performing the logical *AND* operation for all spectra along path k for the modulation m;
$F = \{f_{ij}\}$, set of slots allocated by the fitting function.

Algorithm 1 is the Image-RCMLSA algorithm. In Line 1, the KSPs between s and d are calculated and stored in the set P. In Lines 2–12, for each path calculated by the KSP algorithm, for each modulation level, the availability matrix A_{uv}^m is calculated; this considers the occupancy matrix S_{uv}, the XT generated by the coupled fibers N_{uv}, the effect of the new allocation on the already established lightpaths D_{uv}^m (Line 6), and the physical distance of path $\delta(p_k)$, which is shorter than the maximum distance $MD_{ij}^m(p_k)$ for an aggregated XT along path p on the jth slot of the ith core and modulation format m (Line 8). Lines 12–14 create path spectrum matrices R_k^m by performing a logical *AND* operation between the availability matrices on all the links of the kth path. These matrices are input to the image processing algorithm (Line 17), which will return a list of parts of the available spectrum L_k^m. Lines 18 and 19 block the request if none of those available parts have enough slots for a new lightpath to be allocated. Otherwise, a fitting policy is used to choose which portion of the spectrum in the set L_k^m will be used (Line 21). Finally, in Lines 22–24, the slots chosen are marked as occupied in S_{uv}.

Algorithm 1: Image-RCMLSA

1: $P = kShortest\,Paths(G, s, d, K)$
2: **for all** $p_k \in P$ **do**
3: **for all** $m \in M$ **do**
4: **for all** $u, v | e_{uv} \in p_k, n_{ij} \in N_{uv}, d_{ij} \in D_{uv}^m$ **do**
5: **for all** i, j **do**
6: **if** $(s_{ij} = 0) \wedge (P - n_{ij} \geq T_m) \wedge (d_{ij} = 0)$
7: **then**
8: **if** $\delta(p_k) \leq MD_{ij}^m(p_k)$ **then**
9: $a_{ij} = 0 | a_{ij} \in A_{uv}^m$
10: **else**
11: $a_{ij} = 1 | a_{ij} \in A_{uv}^m$
12: **for all** $p_k \in P$ **do**
13: **for all** $u, v | e_{uv} \in p_k$ **do**
14: $R_k^m = R_k^m \wedge A_{uv}^m$
15: **for all** $k | p_k \in P$ **do**
16: **for all** $m \in M$ **do**
17: $L_k^m = Image\,Processing(R_k^m)$
18: **if** $\forall k, m | L_k^m | < b_m$ **then**
19: $block(r(s, d, b))$
20: **else**
21: $F = fit(r(s, d, b), p_k, L_k^m)$
22: **for all** $u, v | e_{uv} \in p_k$ **do**
23: **for all** $i, j | f_{ij} \in F$ **do**
24: $s_{ij} = 1 | s_{ij} \in S_{uv}$

The computational complexity of the algorithm depends on the complexity of the image processing algorithm used [29,35], which is $O(p)$ for the two algorithms employed in this paper, with p being the number of pixels in the image, regardless of the shape of the spectrum searched. This value can be translated into the number of slots in all the cores of the network ($c \times s$, with c being the number of cores and s the number of slots in each core). The image processing algorithm runs for a separate time for each modulation m for each candidate path k, resulting in a complexity of $O(kmcs)$. The values of m, c, and s can be considered constant for any given topology, and k is a parameter of the algorithm, which can also be fixed. In a static network scenario, the algorithm will always perform the same number of operations for a fixed k; therefore, for this scenario, the complexity is $O(1)$. This complexity is the lowest one possible, and allows network providers to achieve the same computation time for each run of the algorithm for the same network. Thus, the proposed algorithms add no significant computational complexity on the complexity of the KSP algorithm, executed once in the proposed algorithm, with complexity depending only on the number of network nodes and links.

Four fitting policies are proposed to be used jointly with the image processing algorithms. They select the portion of

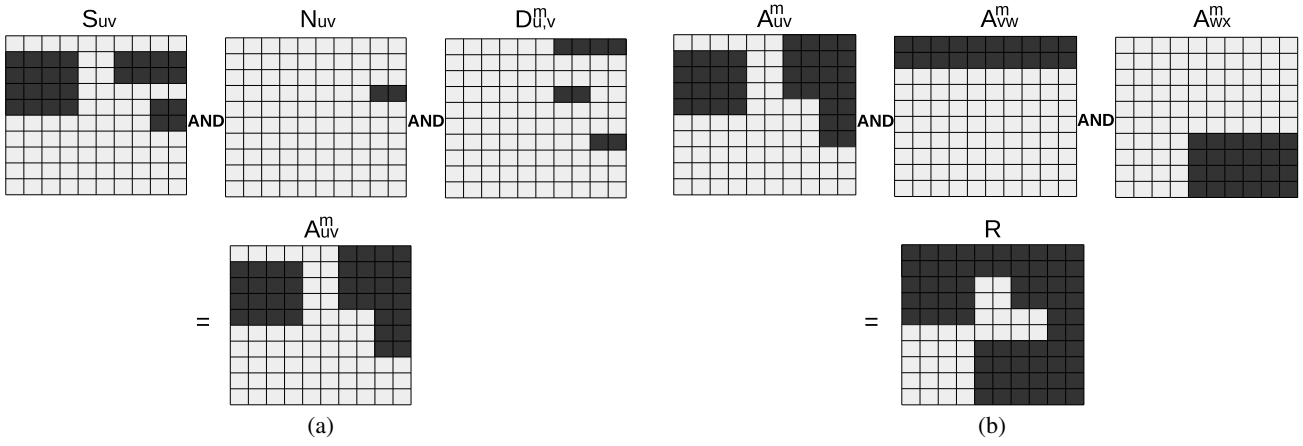

Fig. 3. Matrix calculations. (a) Calculation of the availability matrix and (b) calculation of the path spectrum matrix.

the spectrum in which the lightpath will be allocated. This decision impacts the distribution of the spectrum for the lightpaths and, consequently, the XT they produce with each other. The fitting policies are variations of the traditional best-fit and random-fit policies.

The CCL algorithm identifies regions of the spectrum with arbitrary shapes. Two versions of the CCL algorithm have been proposed, namely, CCL-Best-Fit (CCL-BF) and CCL-Random-Fit (CCL-RF). The IRA algorithm finds only rectangular regions, with height and width being used to derive more elaborate fitting policies. Two IRA-based algorithms are proposed here, namely IRA-Minimal-Blocking (IRA-MB) and IRA-Minimal-Crosstalk (IRA-XT). All four algorithms are described next.

A. CCL-Best-Fit

The CCL-BF algorithm selects the smallest free portions of the spectrum greater than the required bandwidth, thus preventing spectrum fragmentation. This policy minimizes potential spectrum wastage resulting from the availability of non-contiguous slots since these cannot be allocated to incoming requests.

B. CCL-Random-Fit

The CCL-RF algorithm allocates the lightpath to a random region that satisfies the traffic demands, then chooses a random sequence of contiguous slots in that region. This policy distributes the lightpaths better by allowing equal probability of allocation of all portions of the spectrum, thus avoiding possible intercore XT.

C. IRA-Minimal-Blocking

The IRA-MB algorithm is a version of the best fit, which also accounts for the width of a rectangle. The goal of the algorithm is to allocate lightpaths using a single core whenever possible, potentially decreasing the XT, since the spectrum in adjacent cores is not used.

The IRA-MB algorithm chooses the best fitting rectangle by selecting the widest rectangles of the set and the smallest among those.

D. IRA-Minimal-Crosstalk

The IRA-XT algorithm is based on the random-fit policy, which focuses on mitigating XT. However, its random approach can lead to undesirable behavior, causing unexpected high blocking probabilities.

The IRA-XT algorithm uses a random weighted function to allocate a request, with the weight given by the width of the rectangle. This equation allows allocations in a single core whenever possible, thus preventing undesirable allocations.

The algorithms presented and the policies adopted will be evaluated and compared in the section below.

VI. Numerical Evaluation

To assess the performance of the proposed algorithms, simulations were performed with the four algorithms. The parameter $k = 5$ was used in the KSP algorithm since no significant gains were observed using higher values. The FlexGridSim [36] simulator was used for the simulations. Each replication simulated 1,00,000 requests. Confidence intervals with a 95% confidence level were generated. The bandwidth demands of lightpath requests were selected randomly from a discrete uniform distribution {40 Gbps, 100 Gbps, 400 Gbps, and 1 Tbps}. The value of the traffic load was varied by changing the inter-arrival time of the requests. The assumed optical network employed space-wavelength granularity, with multiple input multiple output (MIMO) transceivers and spatially flexible re-configurable optical add/drop multiplexers capable of wavelength-selective switch [37].

The ILP formulation proposed in Ref. [22] was implemented, and the results derived were compared with those obtained with the proposed algorithms. Although its employment in real-world scenarios may not be feasible due to its high computational complexity, this ILP formulation was chosen since it considers modulation levels, thus allowing fair comparison with the proposed algorithms. The ILP was, however, designed for static network scenarios. It was thus solved at the arrival of each request in the dynamic scenario adopted in this paper. The input to the ILP was the set of established lightpaths plus the new request for lightpath establishment. If the solution given by the ILP indicated the feasibility of the allocation of all of the requests, the new lightpath was allocated; otherwise the request was blocked. Rerouting of already established lightpaths was considered in the ILP solution.

The National Science Foundation (NSF) (Fig. 4) and USA (Fig. 5) topologies were used in the simulations. The NSF topology had 16 nodes and 25 links, whereas the USA topology had 24 nodes and 43 links, and thus higher node connectivity. The links were composed of MCFs of

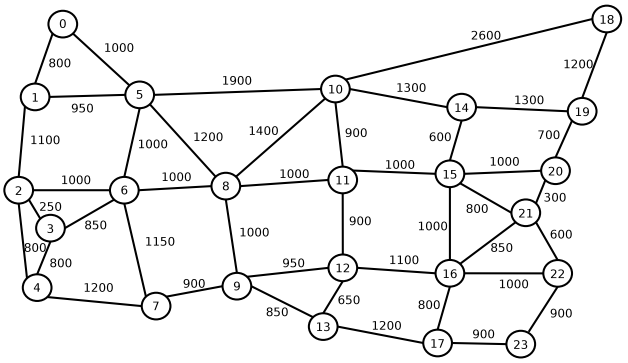

Fig. 4. NSF topology.

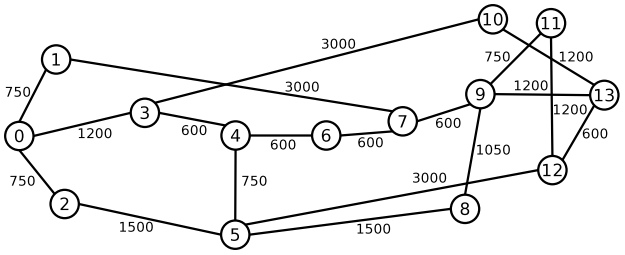

Fig. 5. USA topology.

seven cores, with each core divided into 240 slots of 12.5 GHz each [38]. Requests were dynamically generated by randomly selecting source and destination pairs.

The results of the simulations are presented in two subsections. In the first, the results obtained by the proposed algorithms are compared with those of the ILP for networks with seven cores. In the second, the issue of scaling was evaluated, with the algorithm presenting the best performance being used to compare the results obtained for three different multicore architectures (7, 12, and 19 cores).

Three metrics were evaluated: bandwidth blocking ratio (BBR), which shows the amount of bandwidth blocked over the amount of bandwidth requested; average XT, which was obtained by calculating the average XT affecting all slots of a fiber; average bits per symbol (bps), which is the average number of bits per symbol of the established lightpaths on the network, representing the average modulation level used.

A. Comparison of the Algorithms

The following figures show the results obtained by employing a seven-core fiber architecture, as proposed in Ref. [9]. Figure 6 shows the BBR for the USA topology. All proposed algorithms present lower BBRs than those presented by the ILP baseline algorithm under loads lower than 400 erlangs. Under loads of 200 erlangs, the CCL-RA algorithm produced the lowest BBR values; these are three orders of magnitude lower than those obtained by the ILP and two orders of magnitude lower than those of the other proposed algorithms. As the load increases, the CCL-RA algorithm is affected by the random choices, and the BBR values increase faster than the BBR values given by the other proposed algorithms. Under loads of 350 erlangs, the CCL-BF blocks fewer requests, producing BBR values one order of magnitude lower than the BBRs given by the ILP as well as the other proposed algorithms.

The IRA-XT produces BBR values between those given by the CCL-RA and the CCL-BF, blocking requests two orders of magnitude lower than does the ILP under low loads, and producing BBR values one order of magnitude lower under high load. The IRA-XT, however, produces the most stable results under all loads, with BBR values two orders of magnitude lower than those of the ILP under loads lower than 250 erlangs and one order of magnitude lower for loads greater than 300 erlangs. This is as a consequence of the random spread of the lightpaths over the spectrum with a consequent reduction in XT and higher modulation levels.

Figure 7 shows the BBR values for the NSF topology. The lower node connectivity of this topology results in fewer alternative paths. The proposed algorithms still manage to produce lower BBR values than the ILP under all loads; however, as there are fewer available resources, the BBR values produced by the proposed algorithms are more similar as long as the load is low. The IRA-XT produces BBR values two orders of magnitude lower under loads less than 150 erlangs and one order of magnitude lower under loads less than 150 erlangs, when compared with the BBR values produced by the ILP. These results indicate that the algorithm is able to reduce blocking and maintain the ability to spread the lightpaths over the spectrum, reducing the XT.

The BBR values obtained with the proposed algorithms are generally lower than those of the ILP. This difference is due to the adjustment of modulation as a function of XT on the spectrum slots at the time of the allocation, as well as the spectrum fitting policies used by these algorithms. The CCL-based algorithms employ an aggressive spectrum allocation. The CCL-RA algorithm fails to maintain low XT under high loads, leading to a lower modulation level and

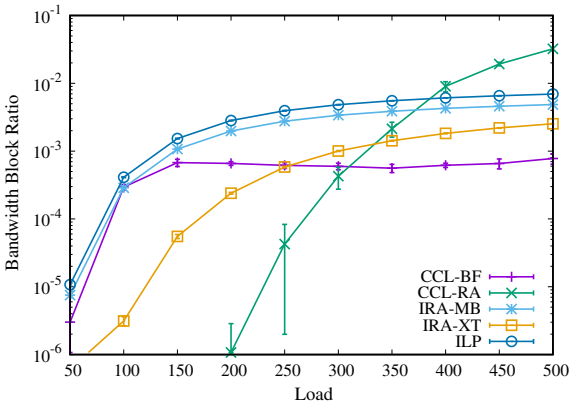

Fig. 6. BBR as a function of load for the USA topology.

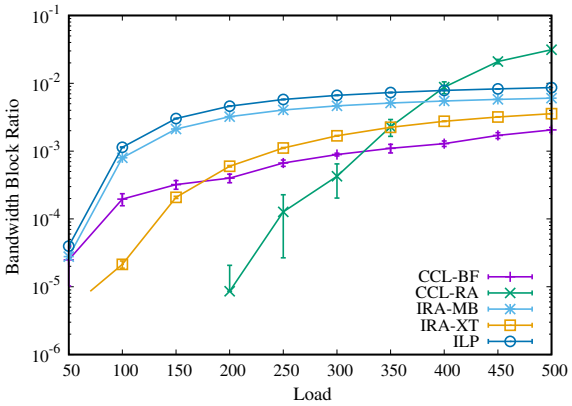

Fig. 7. BBR as a function of load for the NSF topology.

high blocking ratios. The IRA-based algorithms are able to reduce XT by allocating the spectrum in rectangles and using their shapes to fit allocations onto specific portions of the spectrum.

Figure 8 shows the average XT on the network fibers for the USA topology. The average XT produced by the algorithms whose fitting policies consider the XT is less than those of the algorithms that do not consider the XT. Under low loads, the XT produced by IRA-XT and CCL-RA are up to 63 dB lower than those given by the ILP and up to 53 dB lower than those produced by the algorithms that do not aim at minimizing the XT. As the load increases, so does the XT, because the available spectrum without coupled fibers becomes scarce. Under loads of 500 erlangs, the XT values of the CCL-RA are very close to those of the other algorithms, due to saturation of the spectrum; the IRA-XT produces the lowest XT values under 500 erlangs.

Figure 9 shows the average XT for the NSF topology. The results obtained are similar to those of the USA topology; however, since there are fewer available resources, the IRA-XT algorithm produces XT values lower than those obtained by the CCL-RA. The consideration of the width of the rectangles is an efficient approach for reducing XT; this is especially beneficial under high loads, when the spectrum becomes saturated.

The results indicate that the mitigation of XT is more effective in scenarios with high loads, since there are fewer available resources, which makes it difficult to avoid the allocation of lightpaths that generate XT. The consideration of XT during allocation is useful to maintain a low XT, and allows employing high modulation levels, which leads to high spectrum efficiency.

The final aspect of the algorithm to be analyzed is the average bps allocated. The results for the USA topology are shown in Fig. 10. The ILP indicates an almost constant bps, since a previously calculated modulation level based on the distance of the lightpath is used. This leads to high XT values, and, at high loads, affects the spectrum availability. Since the ILP cannot adjust the modulation under high XT values, requests tend to be blocked.

The proposed algorithms decrease the average bps as the load increases. The CCL-RA algorithm is the most affected one, since it employs an aggressive XT minimization. This saturates the spectrum at high loads, with bps values dropping from 4.8 under loads of 50 erlangs to 3.2 under loads of 400 erlangs. The IRA-XT algorithm, on the other hand, is less affected and the bps is the highest. In this case, the average bps decreases from 4.9 under 50 erlangs to 3.9 under 500 erlangs. The average bps results are consistent with the BBR results. In fact, the IRA-XT algorithm blocks fewer requests under high loads, since it allocates lightpaths with higher modulation levels.

Figure 11 shows the average bps allocated for the NSF topology. For this topology, the values obtained by the proposed algorithms are similar to those obtained for the USA topology, due to the lower availability of network resources. Moreover, the results are similar to those obtained for the USA topology, in which the CCL-RA algorithm reduced the average bps under high loads, whereas the IRA-XT algorithm produced the highest bps values under all loads.

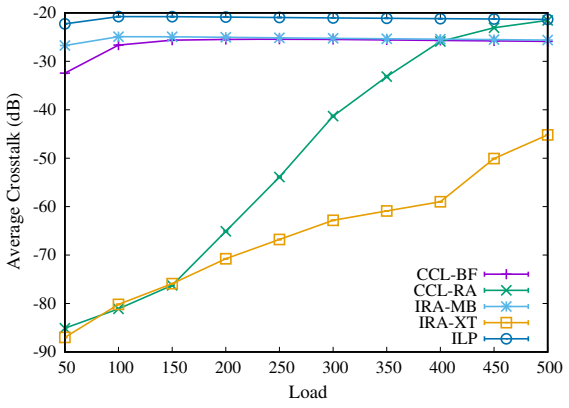

Fig. 8. Average XT of network fibers as a function of load for the USA topology.

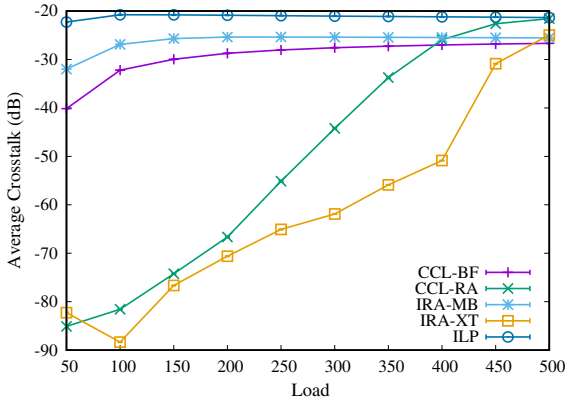

Fig. 9. Average XT of network fibers as a function of load for the NSF topology.

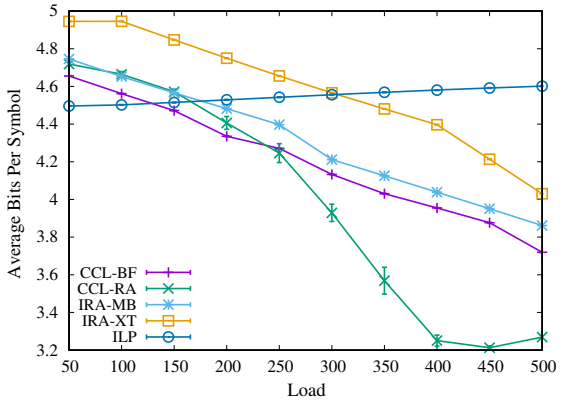

Fig. 10. Average bits per symbol of lightpaths as a function of load for the USA topology.

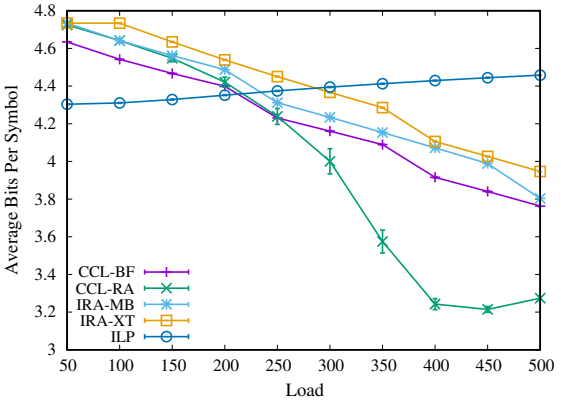

Fig. 11. Average bits per symbol of lightpaths as a function of load for the NSF topology.

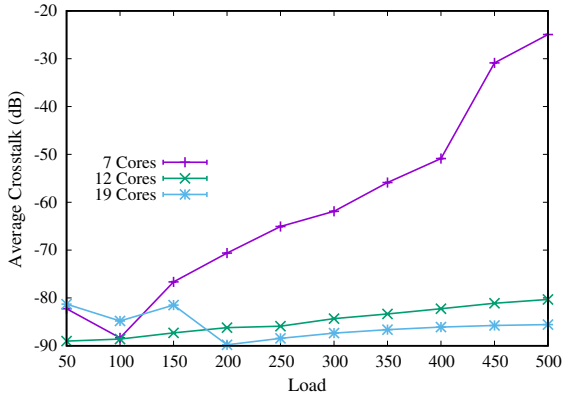

Fig. 13. Average XT of network fibers for different multicore fibers as a function of load for the USA topology.

B. Evaluation of Multi-core Scaling

Given the superior performance of the IRA-XT algorithm in the generated BBR results, independent of the load, this algorithm is evaluated for three multicore architectures.

Figure 12 shows the BBRs produced for the three architectures. The IRA-XT algorithm starts to block requests under loads of 350 erlangs for the 19-core architecture, with BRR values four orders of magnitude lower than those of the seven-core architecture and three orders of magnitude lower than those of the 12-core architecture. These results indicate the ability of the algorithm to take advantage of the high spectrum availability of architectures with a higher core count, where it is possible to spread the lightpaths across the spectrum and avoid XT.

Figure 13 shows that the XT generated is greater when architectures with a fewer number of cores are employed. This reflects in the low availability of spectrum slots, which makes it difficult to avoid XT between lightpaths. When employed in a seven-core architecture, the IRA-XT algorithm generates a maximum XT of −25 dB under loads of 500 erlangs, as opposed to a XT of −80 dB in a 12-core architecture and −85 dB in a 19-core one. These results indicate that the IRA-XT algorithm benefits from a higher availability of spectrum as it generates low XT under these circumstances.

Figure 14 shows the average bps for the three architectures. For a seven-core architecture, the IRA-XT algorithm is forced to lower the modulation level especially as the load increases, since there are fewer slots to be allocated and, consequently, higher average XT. The average bps decreases from 4.7 bps under loads of 50 erlangs to 3.9 bps under loads of 500 erlangs. This decrease is less for the 19-core architecture, for which the value reduces from 4.7 to 4.6 bps. These results show that the spectrum availability of a larger number of cores can be better utilized using a higher modulation level, due to lower average XT.

The IRA-XT algorithm benefits from the high spectrum availability of multiple cores, since it can accommodate a higher number of lightpaths with lower XT, and allocates lightpaths with high modulation level, leading to less blocking of requests.

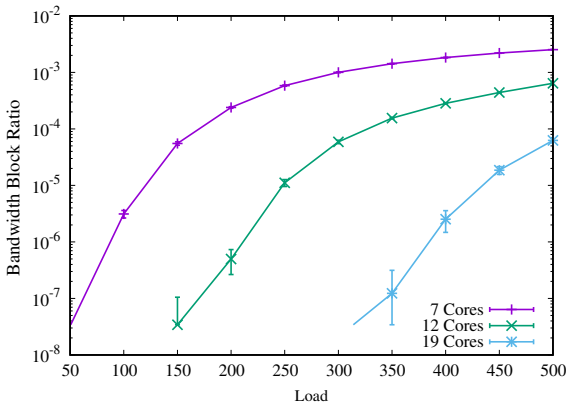

Fig. 12. BBR for different multicore fibers as a function of load for the USA topology.

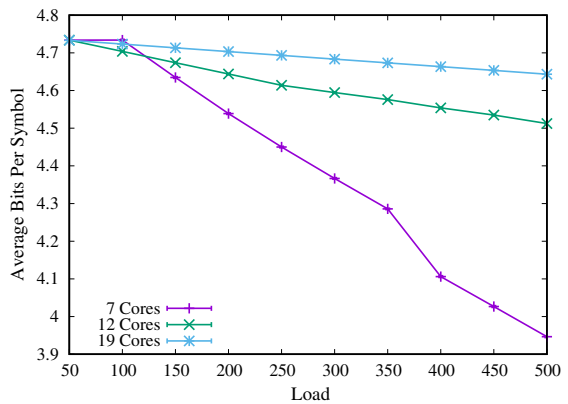

Fig. 14. Average bits per symbol of lightpaths for different multicore fibers as a function of load for the USA topology.

VII. Conclusions

This paper introduced four RCMLSA algorithms based on two different image processing algorithms. These algorithms represent the spectrum availability as a binary image and apply an image processing algorithm to find the available spectrum, thus resulting in an approach with low computational complexity. The two image processing algorithms studied in this paper were the CCL and IRA algorithms. Four fitting policies composed the algorithms that allocate the requests in the available spectrum by considering different parameters such as XT and available spectrum shape. Modulation levels considering the current XT on the cores are employed for efficient allocation of lightpaths on the spectrum.

The results showed that the proposed algorithms can achieve four orders of magnitude lower blocking than that with the baseline ILP. They also indicate that the two image processing algorithms, when used jointly with the four fitting policies to mitigate XT, result in better spectrum efficiency under high resource availability, as in the case of topologies with high node connectivity and core architectures with a large number of cores, since the algorithm can allocate a larger number of lightpaths with low XT values and consequently a high modulation level. Even when spectrum availability is low, the four algorithms are more effective than the baseline ILP.

Acknowledgment

This work was sponsored by Coordenação de Aperfeiçoamento de Pessoal de Nível Superior (CAPES), Conselho Nacional de Desenvolvimento Científico e Tecnológico (CNPq), and São Paulo Research Foundation (FAPESP) grant #15/24494-8, Brazil.

References

[1] X. Chen, A. Jukan, A. C. Drummond, and N. L. S. da Fonseca, "A multipath routing mechanism in optical networks with extremely high bandwidth requests," in *IEEE Global Telecommunications Conf. (GLOBECOM)*, 2009, pp. 1–6.

[2] K. Christodoulopoulos, I. Tomkos, and E. Varvarigos, "Elastic bandwidth allocation in flexible OFDM-based optical networks," *J. Lightwave Technol.*, vol. 29, pp. 1354–1366, 2011.

[3] P. M. Moura, R. A. Scaraficci, and N. L. S. da Fonseca, "Algorithm for energy efficient routing, modulation and spectrum assignment," in *IEEE Int. Conf. on Communications (ICC)*, 2015, pp. 5961–5966.

[4] P. M. Moura, N. L. S. da Fonseca, and R. A. Scaraficci, "Traffic grooming of batches of deadline-driven requests in elastic optical networks," in *IEEE Global Communications Conf.*, 2014, pp. 1284–1289.

[5] S. Fujii, Y. Hirota, H. Tode, and K. Murakami, "On-demand spectrum and core allocation for reducing crosstalk in multicore fibers in elastic optical networks," *J. Opt. Commun. Netw.*, vol. 6, pp. 1059–1071, 2014.

[6] T. Xia, H. Fevrier, T. Wang, and T. Morioka, "Introduction of spectrally and spatially flexible optical networks," *IEEE Commun. Mag.*, vol. 53, no. 2, pp. 24–33, 2015.

[7] D. Klonidis, F. Cugini, O. Gerstel, M. Jinno, V. Lopez, E. Palkopoulou, M. Sekiya, D. Siracusa, G. Thouenon, and C. Betoule, "Spectrally and spatially flexible optical network planning and operations," *IEEE Commun. Mag.*, vol. 53, no. 2, pp. 69–78, 2015.

[8] R. Proietti, L. Liu, R. Scott, B. Guan, C. Qin, T. Su, F. Giannone, and S. Yoo, "3D elastic optical networking in the temporal, spectral, and spatial domains," *IEEE Commun. Mag.*, vol. 53, no. 2, pp. 79–87, 2015.

[9] J. Sakaguchi, Y. Awaji, N. Wada, A. Kanno, T. Kawanishi, T. Hayashi, T. Taru, T. Kobayashi, and M. Watanabe, "Space division multiplexed transmission of 109-Tb/s data signals using homogeneous seven-core fiber," *J. Lightwave Technol.*, vol. 30, pp. 658–665, 2012.

[10] J. Sakaguchi, W. Klaus, B. J. Puttnam, J. M. D. Mendinueta, Y. Awaji, N. Wada, Y. Tsuchida, K. Maeda, M. Tadakuma, K. Imamura, R. Sugizaki, T. Kobayashi, Y. Tottori, M. Watanabe, and R. V. Jensen, "19-core MCF transmission system using EDFA with shared core pumping coupled via free-space optics," *Opt. Express*, vol. 22, pp. 90–95, 2014.

[11] A. Sano, H. Takara, T. Kobayashi, H. Kawakami, H. Kishikawa, T. Nakagawa, Y. Miyamoto, Y. Abe, H. Ono, K. Shikama, M. Nagatani, T. Mori, Y. Sasaki, I. Ishida, K. Takenaga, S. Matsuo, K. Saitoh, M. Koshiba, M. Yamada, H. Masuda, and T. Morioka, "409-Tb/s + 409-Tb/s crosstalk suppressed bidirectional MCF transmission over 450 km using propagation-direction interleaving," *Opt. Express*, vol. 21, pp. 16777–16783, 2013.

[12] L. R. Costa, G. N. Ramos, and A. C. Drummond, "Leveraging adaptive modulation with multi-hop routing in elastic optical networks," *Comput. Netw.*, vol. 105, pp. 124–137, 2016.

[13] C. Rottondi, M. Tornatore, A. Pattavina, and G. Gavioli, "Routing, modulation level, and spectrum assignment in optical metro ring networks using elastic transceivers," *J. Opt. Commun. Netw.*, vol. 5, pp. 305–315, 2013.

[14] X. Chen, Y. Zhong, and A. Jukan, "Multipath routing in elastic optical networks with distance-adaptive modulation formats," in *IEEE Int. Conf. on Communications (ICC)*, 2013, pp. 3915–3920.

[15] X. Luo, X. Chen, and L. Wang, "Energy efficient manycast routing, modulation level and spectrum assignment in elastic optical networks for smart city applications," in *Algorithms and Architectures for Parallel Processing*, S. Ibrahim, K.-K. R. Choo, Z. Yan, and W. Pedrycz, Eds. Cham, Switzerland: Springer, 2017, pp. 633–641.

[16] S. Bandyopadhyay, V. Dey, M. Chatterjee, and U. Bhattacharya, "SEMRSA: spectrum efficient modulation-aware dynamic routing & spectrum allocation in elastic optical network," in *8th Int. Conf. on Computer Modeling and Simulation (ICCMS)*, 2017, pp. 170–174.

[17] Y. Tan, H. Yang, R. Zhu, Y. Zhao, J. Zhang, Z. Liu, Q. Ou, and Z. Zhou, "Distance adaptive routing, core and spectrum allocation in space division multiplexing optical networks with multi-core fibers," in *Asia Communications and Photonics Conf.*, 2016, paper AF2A.159.

[18] H. Tode and Y. Hirota, "Routing, spectrum, and core and/or mode assignment on space-division multiplexing optical networks," *J. Opt. Commun. Netw.*, vol. 9, pp. A99–A113, 2017.

[19] C. Rottondi, P. Martelli, P. Boffi, L. Barletta, and M. Tornatore, "Modulation format, spectrum and core assignment in a multicore flexi-grid optical link," in *Optical Fiber Communications Conf. and Exposition (OFC)*, 2018, pp. 1–3.

[20] M. Klinkowski, P. Lechowicz, and K. Walkowiak, "A study on the impact of inter-core crosstalk on SDM network

performance," in *Int. Conf. on Computing, Networking and Communications (ICNC)*, 2018, pp. 404–408.

[21] M. Yang, Y. Zhang, and Q. Wu, "Routing, spectrum, and core assignment in SDM-EONs with MCF: node-arc ILP/MILP methods and an efficient XT-aware heuristic algorithm," *J. Opt. Commun. Netw.*, vol. 10, pp. 195–208, 2018.

[22] J. Perelló, J. M. Gené, A. Pagès, J. A. Lazaro, and S. Spadaro, "Flex-grid/SDM backbone network design with inter-core XT-limited transmission reach," *J. Opt. Commun. Netw.*, vol. 8, pp. 540–552, 2016.

[23] M. Koshiba, K. Saitoh, K. Takenaga, and S. Matsuo, "Analytical expression of average power-coupling coefficients for estimating intercore crosstalk in multicore fibers," *IEEE Photon. J.*, vol. 4, pp. 1987–1995, 2012.

[24] A. Muhammad, G. Zervas, D. Simeonidou, and R. Forchheimer, "Routing, spectrum and core allocation in flex-grid SDM networks with multi-core fibers," in *Int. Conf. on Optical Network Design and Modeling*, 2014, pp. 192–197.

[25] P. M. Moura and N. L. S. da Fonseca, "Routing, core and spectrum assignment based on connected component labelling for SDM optical networks," in *IEEE Int. Conf. on Communications (ICC)*, 2016, pp. 1–6.

[26] P. M. Moura and N. L. S. da Fonseca, "Inscribed rectangles algorithm for routing, core and spectrum assignment for SDM optical networks," in *IEEE Int. Conf. on Communications (ICC)*, 2017, pp. 1–6.

[27] P. Lechowicz, K. Walkowiak, and M. Klinkowski, "Selection of spectral-spatial channels in SDM flexgrid optical networks," in *Int. Conf. on Optical Network Design and Modeling (ONDM)*, 2017, pp. 1–6.

[28] R. C. Gonzalez and R. E. Woods, *Digital Image Processing*, 3rd ed., Upper Saddle River, New Jersey: Prentice-Hall, 2006.

[29] K. Wu, E. Otoo, and K. Suzuki, "Optimizing two-pass connected-component labeling algorithms," *Pattern Anal. Appl.*, vol. 12, pp. 117–135, 2009.

[30] A. Abubaker, R. Qahwaji, S. Ipson, and M. Saleh, "One scan connected component labeling technique," in *IEEE Int. Conf. on Signal Processing and Communications (ICSPC)*, 2007, pp. 1283–1286.

[31] L. He, Y. Chao, K. Suzuki, and K. Wu, "Fast connected-component labeling," *Pattern Recogn.*, vol. 42, pp. 1977–1987, 2009.

[32] A. Sarkar, A. Biswas, M. Dutt, and A. Bhattacharya, "Finding a largest rectangle inside a digital object and rectangularization," *J. Comput. Syst. Sci.*, vol. 95, pp. 204–217, 2018.

[33] J. Chen, G. Bai, S. Liang, and Z. Li, "Automatic image cropping: a computational complexity study," in *IEEE Conf. on Computer Vision and Pattern Recognition (CVPR)*, 2016, pp. 507–515.

[34] R. J. Essiambre, G. Kramer, P. J. Winzer, G. J. Foschini, and B. Goebel, "Capacity limits of optical fiber networks," *J. Lightwave Technol.*, vol. 28, pp. 662–701, 2010.

[35] L. He, Y. Chao, and K. Suzuki, "A run-based two-scan labeling algorithm," in *Image Analysis and Recognition*, M. Kamel and A. Campilho, Eds., vol. 4633 of Lecture Notes in Computer Science, Heidelberg, Berlin: Springer, 2007, pp. 131–142.

[36] P. M. Moura and A. C. Drummond, "FlexGridSim: flexible grid optical network simulator," [Online]. Available: http://www.lrc.ic.unicamp.br/FlexGridSim/.

[37] D. M. Marom, P. D. Colbourne, A. D'errico, N. K. Fontaine, Y. Ikuma, R. Proietti, L. Zong, J. M. Rivas-Moscoso, and I. Tomkos, "Survey of photonic switching architectures and technologies in support of spatially and spectrally flexible optical networking [invited]," *J. Opt. Commun. Netw.*, vol. 9, pp. 1–26, 2017.

[38] K. Igarashi, K. Takeshima, T. Tsuritani, H. Takahashi, S. Sumita, I. Morita, Y. Tsuchida, M. Tadakuma, K. Maeda, T. Saito, K. Watanabe, K. Imamura, R. Sugizaki, and M. Suzuki, "110.9-Tbit/s SDM transmission over 6,370 km using a full C-band seven-core EDFA," *Opt. Express*, vol. 21, pp. 18053–18060, 2013.

Pedro Mesquita Moura is currently a Ph.D. candidate at the Institute of Computing, University of Campinas (UNICAMP), Brazil. He received his B.Sc. degree in Computer Science from the Federal University of Lavras (UFLA), Brazil, in 2011 and a M.Sc. degree in Computer Science from the University of Campinas, Brazil, in 2015. His research interests include optical networks, routing, energy efficiency, and wireless networks.

Nelson Luis Saldanha da Fonseca received his Ph.D. in Computer Engineering from the University of Southern California, Los Angeles, California, USA, in 1994. He is currently a Full Professor with the Institute of Computing, State University of Campinas, Campinas, Brazil. He has authored or coauthored over 400 papers and has supervised over 60 graduate students. He is currently the Vice President of Technical and Educational Activities of the IEEE Communications Society (ComSoc). He served as the ComSoc Vice President of Publications, Vice President of Member Relations, Director of Conference Development, Director of Latin America Region, and Director of On-Line Services. He is the former Editor-in-Chief of IEEE Communications Surveys and Tutorials. He is a Senior Editor of the IEEE Communications Magazine, and an Editorial Board Member of Computer Networks, and Peer-to-Peer Networking and Applications. He was a recipient of the 2012 IEEE Communications Society (ComSoc) Joseph LoCicero Award for Exemplary Service to Publications, the Medal of the Chancellor of the University of Pisa in 2007, and the Elsevier Computer Network Journal Editor of Year 2001 Award.